AIP | Journal of Applied Physics

Thin film contact resistance with dissimilar materials

Peng Zhang, Y. Y. Lau, and R. M. Gilgenbach

Citation: J. Appl. Phys. **109**, 124910 (2011); doi: 10.1063/1.3596759
View online: http://dx.doi.org/10.1063/1.3596759
View Table of Contents: http://jap.aip.org/resource/1/JAPIAU/v109/i12
Published by the AIP Publishing LLC.

Thin film contact resistance with dissimilar materials

Peng Zhang, Y. Y. Lau,[a] and R. M. Gilgenbach
Department of Nuclear Engineering and Radiological Sciences, University of Michigan, Ann Arbor, Michigan 48109-2104, USA

(Received 3 February 2011; accepted 30 April 2011; published online 28 June 2011)

This paper presents results of thin film contact resistance with dissimilar materials. The model assumes arbitrary resistivity ratios and aspect ratios between contact members, for both Cartesian and cylindrical geometries. It is found that the contact resistance is insensitive to the resistivity ratio for $a/h < 1$, but is rather sensitive to the resistivity ratio for $a/h > 1$ where a is the constriction size and h is film thickness. Various limiting cases are studied and validated with known results. Accurate analytical scaling laws are constructed for the contact resistance over a large range of aspect ratios and resistivity ratios. Typically the minimum contact resistance is realized with $a/h \sim 1$, for both Cartesian and cylindrical cases. Electric field patterns are presented, showing the crowding of the field lines in the contact region. © *2011 American Institute of Physics*.
[doi:10.1063/1.3596759]

I. INTRODUCTION

Thin film contact is a very important issue in many areas, such as integrated circuits,[1,2] thin film devices,[3,4] carbon nanotube and carbon nanofiber based cathodes[5,6] and interconnects,[5,7] field emitters,[6,8] and thin film-to-bulk contacts,[9] etc. Even in the simplest form, the film resistor remains the most fundamental component of various types of circuits.[3,4] Recently, it becomes increasingly important in the miniaturization of electronic devices such as micro-electromechanical system relays and microconnector systems, where thin metal films of a few microns are typically used to form electrical contacts.[9] In high energy density physics, the electrical contacts between the electrode plates and in Z-pinch wire arrays are crucial for high current delivery.[10]

For decades, the fundamental model of electrical contact has been Holm's classical a-spot theory,[11] which assumes a circular contact region (of zero thickness) between two bulk conductors. The a-spot theory has recently been extended to include the effects of finite bulk radius,[12] of finite thickness of contact "bridge,"[13,14] and of dissimilar materials and contaminants.[15] These prior works are inapplicable to the thin film geometry that is studied in this paper (Figs. 1–3). This is particularly the case when the current is mostly confined to the immediate vicinity of the constriction and flows parallel to the thin film boundary.

The two-dimensional (2D) thin film resistance has been investigated for various patterns in Cartesian geometry.[3] The spreading resistance of three-dimensional (3D) thin film disks is also analyzed.[9,16] These prior works assume a constant and uniform electrical resistivity in all regions. In particular, Timsit[9] analytically calculated the spreading resistance of a circular thin conducting film of thickness h connected to a bulk solid via an a-spot constriction of radius a, but with the assumption that the current density distribution through the a-spot of this film is the same as the known current density distribution through the a-spot in a semi-infinite bulk solid.[9,11,12] Timsit stated that his model is reliable only for $0 < a/h \leq 0.5$.[9] As we shall see, in this paper, we are able to confirm Timsit's results for $0 < a/h \leq 0.5$, and at the same time to extend his results for a/h up to ten [cf., the lowest solid curve in Fig. 10].

Most recently, we developed a simple and accurate analytical model for Figs. 1–3, under the same assumption of *constant and uniform resistivity in all regions*.[17] We determined the condition which minimizes the thin film contact resistance for both Cartesian and cylindrical geometries. Our scaling laws were validated against MAXWELL 3D[18] simulation and against conformal mapping results for the Cartesian geometry (Figs. 1 and 2).

In this paper, we greatly extend the analytic theory of Ref. 17 by allowing the contact members to have an arbitrary ratio in electrical resistivity. Figure 1 shows both Cartesian and cylindrical geometries of the thin film. The current flows inside the base thin film with width (thickness) h and electrical resistivity ρ_2, converging toward the center of the joint region, and feeds into the top channel with half-width

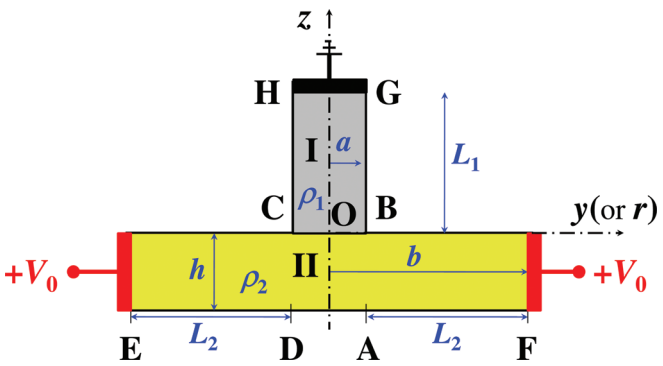

FIG. 1. (Color online) Thin film structures in either Cartesian or cylindrical geometries. Terminals E and F are held at a constant voltage (V_0) relative to terminal GH, which is grounded. The z-axis is the axis of rotation for the cylindrical geometry. The resistivity ratio ρ_1/ρ_2 in Regions I and II is arbitrary.

[a]Electronic mail: yylau@umich.edu.

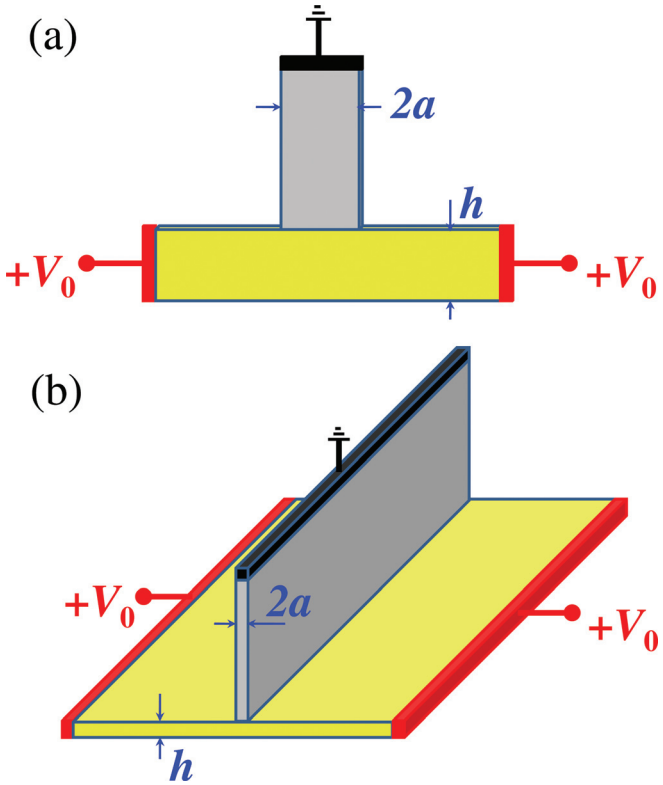

FIG. 2. (Color online) Two cases of Cartesian thin film contact represented by Fig. 1: (a) thin film sheet resistor and (b) heatsink geometry.

(radius) a and electrical resistivity ρ_1, in Cartesian (cylindrical) geometry. This configuration is representative to various applications. The Cartesian case may represent a thin film sheet resistor [Fig. 2(a)],[3] where the third dimension, which is perpendicular to the plane of the paper, is small. It may also represent a heatsink geometry [Fig. 2(b)], where this third dimension is large. The cylindrical case (Fig. 3) may represent a carbon nanotube[5–8] or a field emitter[6] setting on a substrate; or it may represent a z-pinch wire connected to a plate electrode.[10] It is assumed that the axial extent of the top channel (i.e., L_1 in Fig. 1) is so long that the current flow in this region is uniform far from the contact region. Our analytic formulation (given in detail in the Appendices) assume a finite length L_2 in the base region (Fig. 1). Thus, we study the dependence of the contact or constriction resistance on the geometries and resistivities shown in Fig. 1, for arbitrary values of a, b, h, ρ_1, and ρ_2 (Figs. 4, 5, 9, and 10). The potential profiles are formulated exactly, from which the interface contact resistances are derived. Simple, accurate

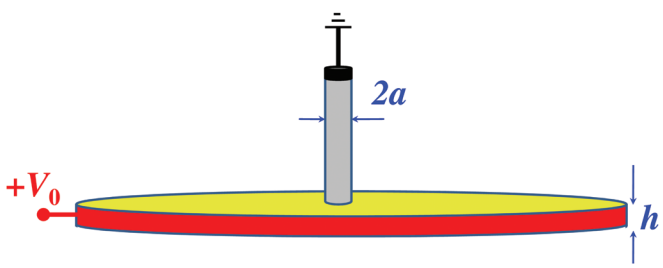

FIG. 3. (Color online) Cylindrical case of thin film contact represented by Fig. 1.

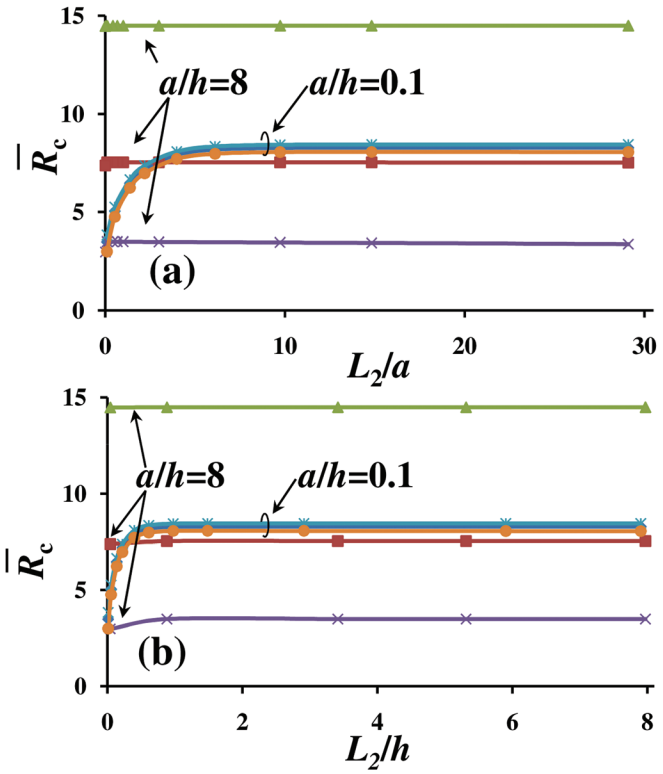

FIG. 4. (Color online) $\bar{R}_c$ for the Cartesian structure in Figs. 1 and 2 is plotted as a function of (a) L_2/a and (b) L_2/h for $a/h = 0.1$ and 8.0, and $\rho_1/\rho_2 = 10$, 1.0, and 0.1 (top to bottom).

scaling laws for the thin film contact resistance are synthesized (Figs. 6 and 11). The patterns of current flow are also displayed. The conditions to minimize the contact resistance are identified in various limits. Validation of our theory against known results is indicated.

Only the major results will be presented in the main text. Their derivations are given in the appendices. In Sec. II,

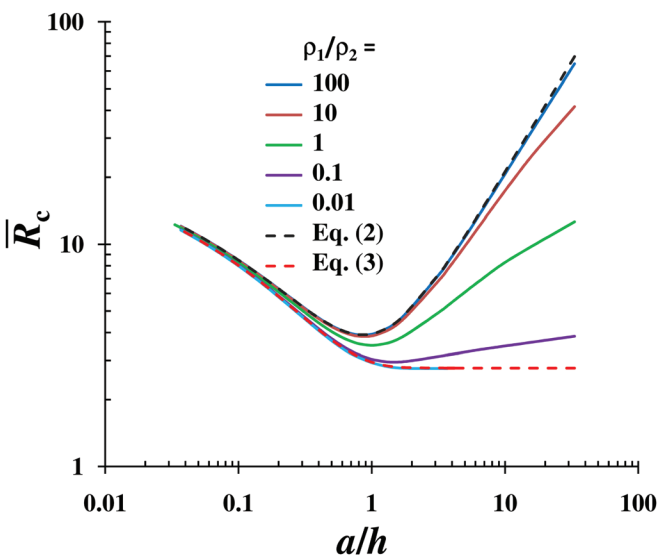

FIG. 5. (Color online) $\bar{R}_c$ as a function of a/h, for the Cartesian structure in Figs. 1 and 2. The solid line represents the exact calculations [Eq. (A8)], where each curve consists of many combinations of b/a and b/h, with either $L_2 \gg a$ or $L_2 \gg h$. The dashed lines represent the limiting cases of $\rho_1/\rho_2 \to \infty$ [Eq. (2)] and $\rho_1/\rho_2 \to 0$ [Eq. (3)].

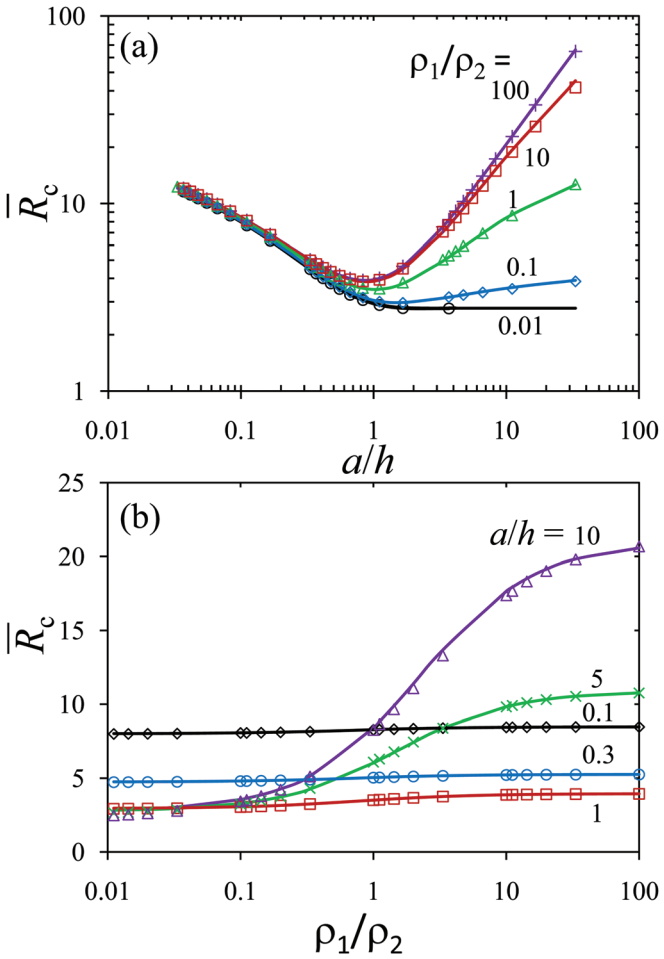

FIG. 6. (Color online) $\bar{R}_c$ for Cartesian thin film structures in Figs. 1 and 2, as a function of (a) aspect ratio a/h and (b) resistivity ratio ρ_1/ρ_2; symbols for the exact theory, solid lines for the scaling law Eq. (4).

the results for the Cartesian thin film contact resistance (constriction resistance) with dissimilar materials are presented [Fig. 2]. In Sec. III, the results for the cylindrical thin film contact resistance (constriction resistance) with dissimilar materials are presented [Fig. 3]. Concluding remarks are given in Sec. IV.

II. CARTESIAN THIN FILM CONTACT WITH DISSIMILAR MATERIALS

Let us first consider the 2D Cartesian "T"-shape thin film pattern (Figs. 1 and 2). The pattern is symmetrical about the vertical center axis. Current flows from the two terminals E, F to the top terminal GH (Fig. 1). We solve the Laplace's equation for Regions I and II, and match the boundary conditions at the interface BC, $z=0$. The details of the calculations are given in the Appendix A. The total resistance, R, from EF to GH is found to be

$$R = \frac{\rho_2 L_2}{2h \times W} + \frac{\rho_2}{4\pi W}\overline{R}_c\left(\frac{a}{b}, \frac{a}{h}, \frac{\rho_1}{\rho_2}\right) + \frac{\rho_1 L_1}{2a \times W}, \qquad (1)$$

where W denotes the channel width in the third, ignorable dimension that is perpendicular to the paper, and the rest of the symbols have been defined in Fig. 1. In Eq. (1), the first term represents the bulk resistance of the thin film base, from A to F, and from D to E, where $L_2 = b - a$. The third term represents the bulk resistance of the top region from B to G. The second term represents the remaining constriction (or contact) resistance, R_c, for the region $ABCD$. If we express the constriction (contact) resistance as $R_c = (\rho_2/4\pi W)\overline{R}_c$ for the Cartesian case, we find that $\overline{R}_c$ depends on the aspect ratios a/h and a/b, and on the resistivity ratio ρ_1/ρ_2, as explicitly shown in Eq. (1). The *exact* expression for $\overline{R}_c$ is derived in Appendix A [cf., Eq. (A8)]. In Eq. (A8), the coefficient B_n is solved numerically in terms of ρ_1/ρ_2, a/h, and a/b [cf., Eq. (A6)]. These numerical values of B_n then give $\overline{R}_c$ from Eq. (A8).

The exact theory of $\overline{R}_c$ [cf., Eq. (A8)] is plotted in Fig. 4(a) as a function of L_2/a, for various ρ_1/ρ_2 and a/h. To explicitly examine the dependence on the geometrical parameters, $\overline{R}_c$ in Fig. 4(a) is replotted as a function of L_2/h in Fig. 4(b). It is seen from Fig. 4 that $\overline{R}_c$ becomes almost a constant if either $L_2/a \gg 1$ or $L_2/h \gg 1$, in which case $\overline{R}_c$ is determined only by the value of a/h and ρ_1/ρ_2, independent of b. Many other similar calculations (not shown) lead to the same conclusion. This is due to the fact that if $L_2 \gg a$, the electrostatic fringe field at the corner B (Fig. 1) is restricted to a distance of at most a few a's, making the flow field at the terminal F insensitive to b. Likewise, if $L_2 \gg h$, the electrostatic fringe field at the corner B is restricted to a distance of at most a few h's, making the flow field at the terminal F also insensitive to b.

In Fig. 5, the exact theory of $\overline{R}_c$ [cf., Eq. (A8)] is plotted as a function of a/h, for various ρ_1/ρ_2. Each solid curve in Fig. 5 consists of many combinations of b/a and b/h, with either $L_2 \gg a$ or $L_2 \gg h$. Again, $\overline{R}_c$ is independent of b, provided either $L_2 \gg a$ or $L_2 \gg h$. For a given a/h, $\overline{R}_c$ increases as ρ_1/ρ_2 increases. It is clear that there exists a minimum of value of $\overline{R}_c$ in the region of a/h near unity, for a given ρ_1/ρ_2. This a/h value for minimum $\overline{R}_c$ decreases slightly as ρ_1/ρ_2 increases. For the special case of $\rho_1/\rho_2 = 1$, the minimum $\overline{R}_c = 2\pi - 4\ln 2 = 3.5106$ occurs exactly at $a/h = 1$,[3,17] and if a/h deviates from 1, $\overline{R}_c$ increases logarithmically as $\overline{R}_c \cong -4\ln(a/h) - 1.5452$ for $a/h \ll 1$, and $\overline{R}_c \cong 4\ln(a/h) - 1.5452$ for $a/h \gg 1$.[3,17] In the regime $a/h < 1$, the range of variation $\overline{R}_c(\rho_1/\rho_2)$ for a given a/h is insignificant (Fig. 5); however, in the regime of $a/h > 1$, $\overline{R}_c(\rho_1/\rho_2)$ for a given a/h may change by an order of magnitude or more.

In the limit of $\rho_1/\rho_2 \to \infty$, $\overline{R}_c$ is simplified as (cf., Eq. (A10) in Appendix A)

$$\overline{R}_c|_{\rho_1/\rho_2 \to \infty} = 4\sum_{n=1}^{\infty} \frac{\coth[(n-1/2)\pi h/b]}{n-1/2} \frac{\sin^2[(n-1/2)\pi a/b]}{[(n-1/2)\pi a/b]^2} - 2\pi(b-a)/h, \qquad (2)$$

which is also plotted in Fig. 5. Note that the exact theory for $\rho_1/\rho_2 = 100$ overlaps with Eq. (2). In the limit of $\rho_1/\rho_2 \to \infty$, the minimum $\overline{R}_c \cong 3.9$ occurs at $a/h = 0.85$, as shown in Fig. 5.

In the opposite limit, $\rho_1/\rho_2 \to 0$, the region $BCHG$ (Fig. 1) acts as a perfectly conducting material with respect to the base region $BCEF$. Thus, the whole constriction

interface BC is an equipotential surface, as if $L_1 = 0$ and the external electrode is applied directly to the interface BC for the Cartesian geometry. This special case is analyzed by Hall (cf., Fig. 2 and Eq. (12) of Hall's 1967 paper[3]), and from which $\bar{R}_c$ in the limit of $\rho_1/\rho_2 \to 0$ is given as

$$\bar{R}_c|_{\rho_1/\rho_2 \to 0} = 2\pi \frac{a}{h} - 4 \ln\left[\sinh\left(\frac{\pi}{2}\frac{a}{h}\right)\right], \tag{3}$$

which is also plotted in Fig. 5. Note that the exact theory for $\rho_1/\rho_2 = 0.01$ overlaps with Eq. (3). This agreement may be considered as one validation of the analytic theory presented in Appendix A. In the limit of $\rho_1/\rho_2 \to 0$, $\bar{R}_c$ converges to a constant minimum value of $4\ln 2 = 2.77$ for $a/h > 2$, as shown in Fig. 5.

As another validation, consider the special case $\rho_1/\rho_2 = 1$ and $L_2 = 0$ (Fig. 1). This case has an exact solution using conformal mapping.[3] The exact values of $\bar{R}_c$ for $a/h = 0.1$ and $a/h = 8$ obtained from conformal mapping are, respectively, 2.77259 and 7.27116. In comparison, our numerical values are, respectively, 2.7722 and 7.2692, as shown in the data for $L_2 = 0$ in Fig. 4.

The vast amount of data collected from the exact calculations allows us to synthesize a simple scaling law for the normalized contact resistance $\bar{R}_c$ in Eq. (1) and Fig. 5 as (for $L_2 \gg a$ or $L_2 \gg h$)

$$\bar{R}_c\left(\frac{a}{h}, \frac{\rho_1}{\rho_2}\right) \cong \bar{R}_{c0}\left(\frac{a}{h}\right) + \frac{\Delta\left(\frac{a}{h}\right)}{2} \times \frac{2\rho_1}{\rho_1 + \beta\left(\frac{a}{h}\right)\rho_2}, \tag{4}$$

$$\bar{R}_{c0}(a/h) = \bar{R}_c(a/h)|_{\rho_1/\rho_2 \to 0} = 2\pi a/h - 4\ln[\sinh(\pi a/2h)], \tag{5}$$

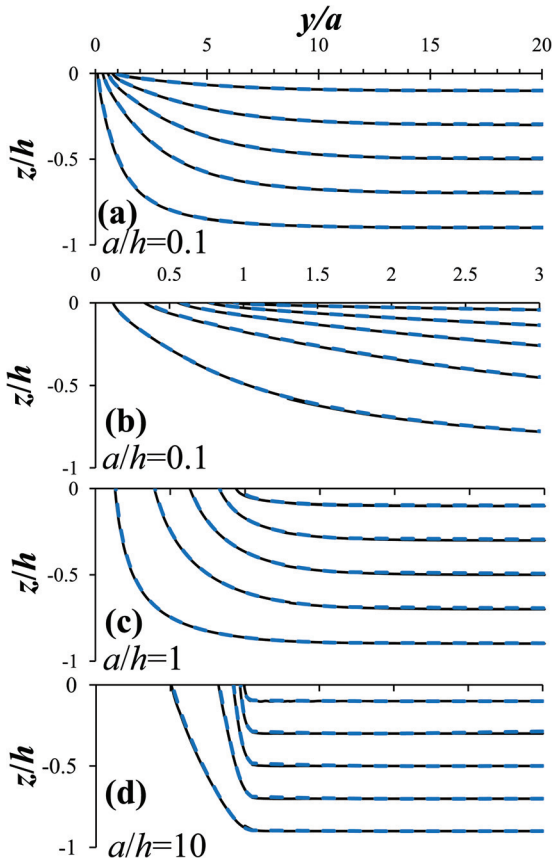

FIG. 7. (Color online) Field lines in the right half of Region II of the Cartesian geometry in Fig. 1 for $\rho_1/\rho_2 = 1$ with (a) $a/h = 0.1$, (b) zoom in view of (a) for $0 \le y/a \le 3$, (c) $a/h = 1$, and (d) $a/h = 10$. The results from series expansion method [Eq. (A1)] (solid lines) are compared to those from conformal mapping (dashed lines).

$$\Delta(a/h) = \begin{cases} 0.5346(a/h)^2 + 0.0127(a/h) + 0.4548, & 0.03 \le a/h \le 1; \\ 0.0147x^6 - 0.0355x^5 + 0.1479x^4 + 0.4193x^3 + 1.1163x^2 + 0.9970x + 1, \\ \quad x = \ln(a/h), 1 < a/h \le 30, \end{cases}$$
$$\beta(a/h) = -0.0003(a/h)^2 + 0.1649(a/h) + 0.6727, \quad 0.03 \le a/h \le 30. \tag{6}$$

This scaling law of Cartesian thin film contact resistance, Eq. (4), is shown in Fig. 6, which compares extremely well with the exact theory, for the range of $0 < \rho_1/\rho_2 < \infty$ and $0.03 \le a/h \le 30$. (We have not found the scaling law for $a/h > 30$ for general values of ρ_1/ρ_2, as data for $a/h > 30$ are not easy to generate from the exact theory, Eq. (A8).)

The field line equation, $y = y(z)$, may be numerically integrated from the first order ordinary differential equation $dy/dz = E_y/E_z = (\partial\Phi_-/\partial y)/(\partial\Phi_-/\partial z)$ where Φ_- is given by Eq. (A1). Figure 7 shows the field lines in the right half of Region II (Fig. 1) for the special case of $\rho_1/\rho_2 = 1$, with various aspect ratios a/h. It is clear that the field lines are most uniformly distributed over the conduction region when $a/h = 1$, which is consistent with the minimum normalized contact resistance $\bar{R}_c$ at $a/h = 1$ for $\rho_1/\rho_2 = 1$ (Fig. 5). The field lines are *horizontally* crowded around the corner of the constriction when $a/h \ll 1$ [Fig. 7(b)], since in this limit most of the potential variations in the thin film (Region II in Fig. 1) are restricted to a distance of a few a's. The field lines become *vertically* crowded around the corner of the constriction when $a/h \gg 1$ [Fig. 7 (d)], since in this limit most of the potential variations in the upper region (Region I in Fig. 1) are restricted to a distance of a few h's. Both limits lead to higher contact resistance in general (Figs. 5 and 6). In Fig. 8, the field lines are shown for the special case of $a/h = 1$, with various resistivity ratios ρ_1/ρ_2. As ρ_1/ρ_2 increases, Region II becomes more conductive relative to Region I, the interface between Region I and II (i.e., BC in Fig. 1) becomes more and more like an equipotential, therefore, the field lines (and the current density) at the interface become more uniformly distributed, as shown in Fig. 8(c). For $\rho_1/\rho_2 = 1$, the calculated field lines [from Eq. (A1)] are also compared to those obtained from conformal mapping, with excellent agreement for all calculations, as shown in Figs. 7 and 8(b). This close agreement of the field lines with the exact conformal mapping formulation is another validation of the series expansion method.

III. CYLINDRICAL THIN FILM CONTACT WITH DISSIMILAR MATERIALS

We now consider the cylindrical configuration of Fig. 1 using a similar approach. A long cylindrical rod of radius a with resistivity ρ_1, is standing on the center of a large thin-film circular disk of thickness h, and radius $b=a+L_2$ with resistivity ρ_2. Current flows inside the thin-film disk from circular rim E and F to terminal GH (Figs. 1 and 3). We solve the Laplace's equation for Regions I and II, and match the boundary conditions at the interface BC, $z=0$. The details of the calculations are given in the Appendix B. The total resistance, R, from EF to GH is found to be

$$R=\frac{\rho_2}{2\pi h}\ln\left(\frac{b}{a}\right)+\frac{\rho_2}{4a}\bar{R}_c\left(\frac{a}{b},\frac{a}{h},\frac{\rho_1}{\rho_2}\right)+\frac{\rho_1 L_1}{\pi a^2}. \qquad (7)$$

In Eq. (7), the first term represents the bulk resistance of the thin film in Region II, exterior to the constriction region $ABCD$. It is simply the resistance of a disk of inner radius a, outer radius b, and thickness h.[9] The third term represents the bulk resistance of the top cylinder, $BCHG$. The second term represents the remaining constriction resistance, R_c, for the region $ABCD$. If we express the constriction (contact) resistance as $R_c=(\rho_2/4a)\bar{R}_c$ for the cylindrical case, we find that $\bar{R}_c$ depends on the aspect ratios a/h and a/b, and on the resistivity ratio ρ_1/ρ_2, as explicitly shown in Eq. (7). The *exact* expression for $\bar{R}_c$ is derived in Appendix B [cf., Eq. (B8)]. In Eq. (B8), the coefficient B_n is solved numerically in terms of ρ_1/ρ_2, a/h, and a/b [cf., Eq. (B6)]. These numerical values of B_n then give $\bar{R}_c$ from Eq. (B8).

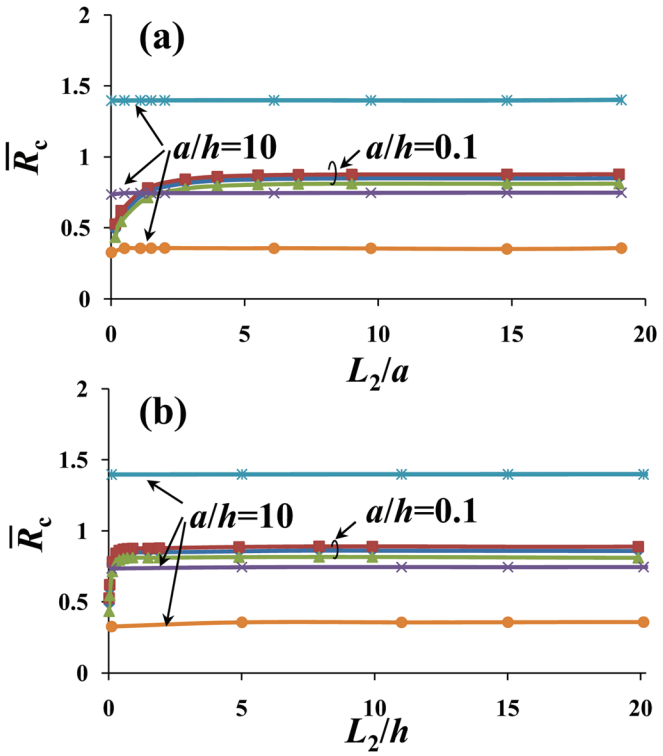

FIG. 9. (Color online) $\bar{R}_c$ for the cylindrical structure in Figs. 1 and 3, is plotted as a function of (a) L_2/a, and (b) L_2/h, for $a/h=0.1$ and 10.0, and $\rho_1/\rho_2=10$, 1.0, and 0.1 (top to bottom).

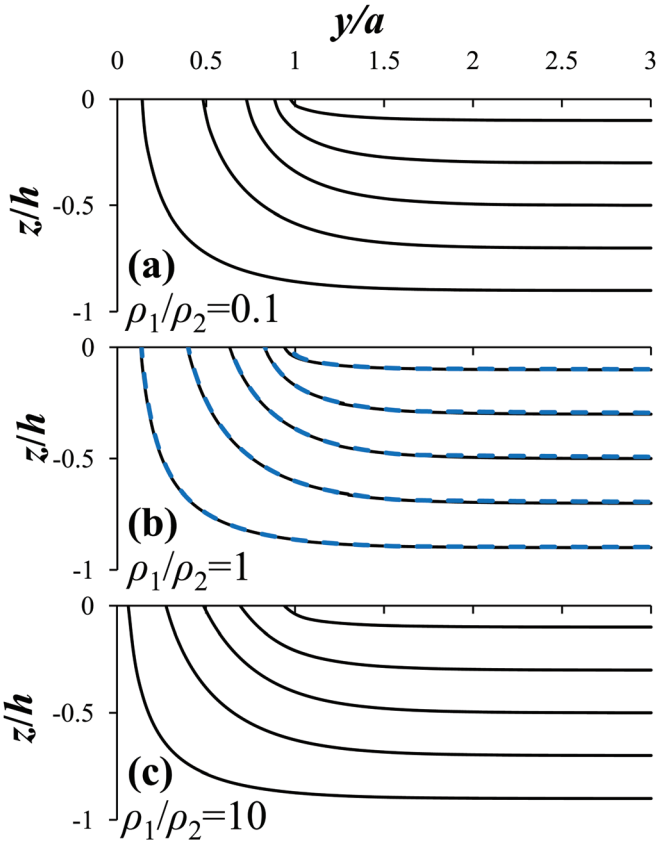

FIG. 8. (Color online) Field lines in the right half of Region II of the Cartesian geometry in Fig. 1 for $a/h=1$ with (a) $\rho_1/\rho_2=0.1$, (b) $\rho_1/\rho_2=1$, and (c) $\rho_1/\rho_2=10$. For $\rho_1/\rho_2=1$, the results from series expansion method [Eq. (A1)] (solid lines) are compared to those from conformal mapping (dashed lines).

The exact theory of $\bar{R}_c$ [Eq. (B8)] is plotted in Fig. 9(a) as a function of L_2/a, for various ρ_1/ρ_2 and a/h, where $L_2=b-a$ (Fig. 1). To explicitly examine the dependence on the geometrical parameters, $\bar{R}_c$ in Fig. 9(a) is replotted as a function of L_2/h in Fig. 9(b). It is found that $\bar{R}_c$ becomes constant if either $L_2/a\gg 1$ or $L_2/h\gg 1$, in which case $\bar{R}_c$ is determined only by the value of a/h and ρ_1/ρ_2, independent of b. Many other similar calculations (not shown) lead to the same conclusion. This is due to the fact that if $L_2\gg a$, the electrostatic fringe field at the corner B (Fig. 1) is restricted to a distance of at most a few a's, making the flow field at the terminal F insensitive to b. Likewise, if $L_2\gg h$, the electrostatic fringe field at the corner B is restricted to a distance of at most a few h's, making the flow field at the terminal F also insensitive to b.

In Fig. 10, the exact theory of $\bar{R}_c$ [cf., Eq. (B8)] is plotted as a function of a/h, for various ρ_1/ρ_2 and a/b. Again, $\bar{R}_c$ is independent of b, provided either $L_2\gg a$ or $L_2\gg h$. For a given a/h, $\bar{R}_c$ increases as ρ_1/ρ_2 increases, similar to the Cartesian case. It is clear that there is a minimum of value of $\bar{R}_c$ in the region of a/h near 1.5, for a given ρ_1/ρ_2. The a/h value for minimum $\bar{R}_c$ decreases slightly as ρ_1/ρ_2 increases. For the special case of $\rho_1/\rho_2=1$, the minimum $\bar{R}_c\cong 0.42$ occurs at $a/h\cong 1.6$.[17] $\bar{R}_c$ is fitted to the following formula for $\rho_1/\rho_2=1$:[17]

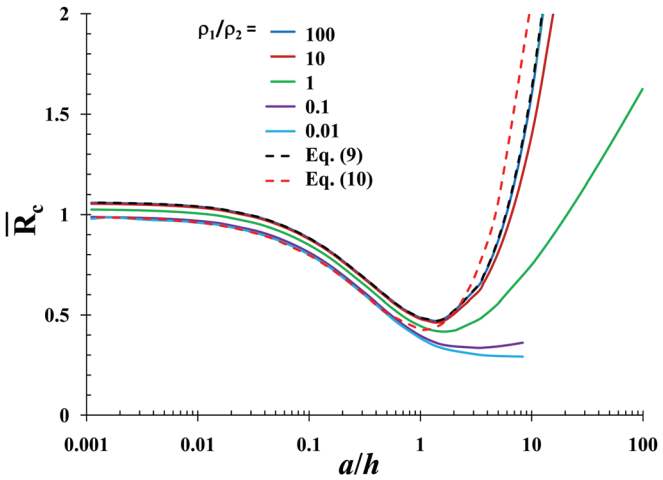

FIG. 10. (Color online) $\bar{R}_c$ as a function of a/h, for the cylindrical structure in Figs. 1 and 3. The solid lines represent the exact calculations [Eq. (B8)], where each curve consists of many combinations of b/a and b/h, with either $L_2 \gg a$ or $L_2 \gg h$. The dashed lines represent the limiting cases of $\rho_1/\rho_2 \to \infty$ [Eq. (9)] and $\rho_1/\rho_2 \to 0$ [Eq. (10)].

$$\bar{R}_c \cong 1.0404 - 2.2328x + 5.0695x^2 - 7.5890x^3 + 6.5898x^4 - 2.9466x^5 + 0.5226x^6, x = a/h, a/h \le 1.6;$$
$$\bar{R}_c \cong 0.4571 - 0.1588y + 0.1742y^2 - 0.0253y^3 + 0.0015y^4, \quad y = \ln(a/h), 1.6 < a/h < 100. \tag{8}$$

In the regime $a/h < 1$, the variation $\bar{R}_c(\rho_1/\rho_2)$ for a given a/h is insignificant; however, in the regime of $a/h > 1$, $\bar{R}_c(\rho_1/\rho_2)$ for a given a/h changes by a factor in the single digits, up to an order of magnitude as shown in Fig. 10. The cylindrical case differs from the Cartesian case in one aspect, namely, as $a/h \to 0$, our numerical calculations show that $\bar{R}_c$ converges to constant values, ranging from about 1 to 1.08, essentially for $0 < \rho_1/\rho_2 < \infty$. The explanation follows. If $a/h \to 0$, both the radius and thickness of the film region are much larger than the radius a of the top cylinder, as if two semi-infinite long cylinders are joining together with radius ratio of $b/a \to \infty$. In this case, the a-spot theory[11] gives a value of $\bar{R}_c$ in the range of 1 to 1.08, for $0 < \rho_1/\rho_2 < \infty$ [c.f., Eq. (2) of Ref. 15].

In the limit of $\rho_1/\rho_2 \to \infty$, $\bar{R}_c$ is simplified as (cf., Eq. (B10) in Appendix B)

$$\bar{R}_c\big|_{\rho_1/\rho_2 \to \infty} = \frac{16}{\pi}\sum_{n=1}^{\infty} \frac{J_1^2(\lambda_n a/b)}{\lambda_n a/b} \frac{\coth(\lambda_n h/b)}{\lambda_n^2 J_1^2(\lambda_n)} - \frac{2a}{\pi h}\ln(b/a), \tag{9}$$

which is also plotted in Fig. 10. Note that the exact theory for $\rho_1/\rho_2 = 100$ overlaps with Eq. (9). In the limit of $\rho_1/\rho_2 \to \infty$, the minimum $\bar{R}_c \cong 0.48$ occurs at $a/h = 1.3$, as shown in Fig. 10.

In the opposite limit, $\rho_1/\rho_2 \to 0$, the region $BCHG$ (Fig. 1) acts as a perfectly conducting material with respect to the base region $BCEF$. Thus, the whole constriction interface BC is an equipotential surface, as if $L_1 = 0$ and the external electrode is applied directly to the interface BC for the cylindrical geometry. This special case is analyzed by Timsit (cf., Fig. 7 and Eq. (18) of Ref. 9), whose $\bar{R}_c$ in the limit of $\rho_1/\rho_2 \to 0$ is

$$\bar{R}_c\big|_{\rho_1/\rho_2 \to 0} = \frac{4}{\pi}\sum_{n=1}^{\infty} \coth(\lambda_n h/b) \frac{\sin(\lambda_n a/b)}{\lambda_n^2 J_1^2(\lambda_n)} - \frac{2a}{\pi h}\ln(b/a). \tag{10}$$

Timsit acknowledges that Eq. (10) is accurate only for the range of $0 < a/h \le 0.5$,[9] beyond which the assumption of equipotential contact that he introduces to derive Eq. (10) does not hold and the result is not accurate anymore. This insight of Timsit and the accuracy of his solution for $a/h < 0.5$ are evident in Fig. 10, where Eq. (10) is plotted. Note that the exact theory for $\rho_1/\rho_2 = 0.01$ overlaps with Eq. (10) up to $a/h = 0.5$. For $a/h > 0.5$, the exact calculation of $\bar{R}_c$ [cf., Eq. (B8)] is also difficult in the limit of $\rho_1/\rho_2 \to 0$, since the determinant of the matrix for solving the coefficient B_n in Eq. (B6) is close to zero. [This is the main reason why the scaling law given in Eq. (11) below is valid only for $a/h \le 10$]. Nevertheless, our calculations of $\bar{R}_c$ for $\rho_1/\rho_2 = 0.01$ shown in Fig. 10 are accurate up to $a/h \le 10$, from the convergence of results as sufficiently large number of terms in the infinite series of Eqs. (B6) and (B8) are employed in our numerical calculations. Thus, our agreement with Timsit's calculations for $a/h < 0.5$ may be considered as a validation of our series expansion method, and we have extended Timsit's calculations[9] to $a/h = 10$ in Fig. 10. We also spot checked our results against the MAXWELL 3D code for the case $\rho_1/\rho_2 = 1$.[17]

The vast amount of data collected from the exact calculations allows us to synthesize a simple scaling law for the normalized contact resistance $\bar{R}_c$ in Eq. (7) and Fig. 10 as (for $L_2 \gg a$ or $L_2 \gg h$)

$$\bar{R}_c\left(\frac{a}{h}, \frac{\rho_1}{\rho_2}\right) \cong \bar{R}_{c0}\left(\frac{a}{h}\right) + \frac{\Delta\left(\frac{a}{h}\right)}{2} \times \frac{2\rho_1}{\rho_1 + \beta\left(\frac{a}{h}\right)\rho_2}, \tag{11}$$

$$\bar{R}_{c0}(a/h) = \bar{R}_c(a/h)\big|_{\rho_1/\rho_2 \to 0} = \begin{cases} 1 - 2.2968(a/h) + 4.9412(a/h)^2 - 6.1773(a/h)^3 \\ +3.811(a/h)^4 - 0.8836(a/h)^5, \quad 0.001 \le a/h \le 1; \\ 0.295 + 0.037(h/a) + 0.0595(h/a)^2, \quad 1 < a/h < 10, \end{cases} \tag{12}$$

$$\Delta(a/h) = \begin{cases} 0.0184(a/h)^2 + 0.0073(a/h) + 0.0808, \quad 0.001 \le a/h \le 1; \\ 0.0409x^4 - 0.1015x^3 + 0.265x^2 - 0.0405x + 0.1065, x = \ln(a/h), \quad 1 < a/h < 10, \end{cases} \tag{13}$$
$$\beta(a/h) = 0.0016(a/h)^2 + 0.0949(a/h) + 0.6983, \quad 0.001 \le a/h < 10.$$

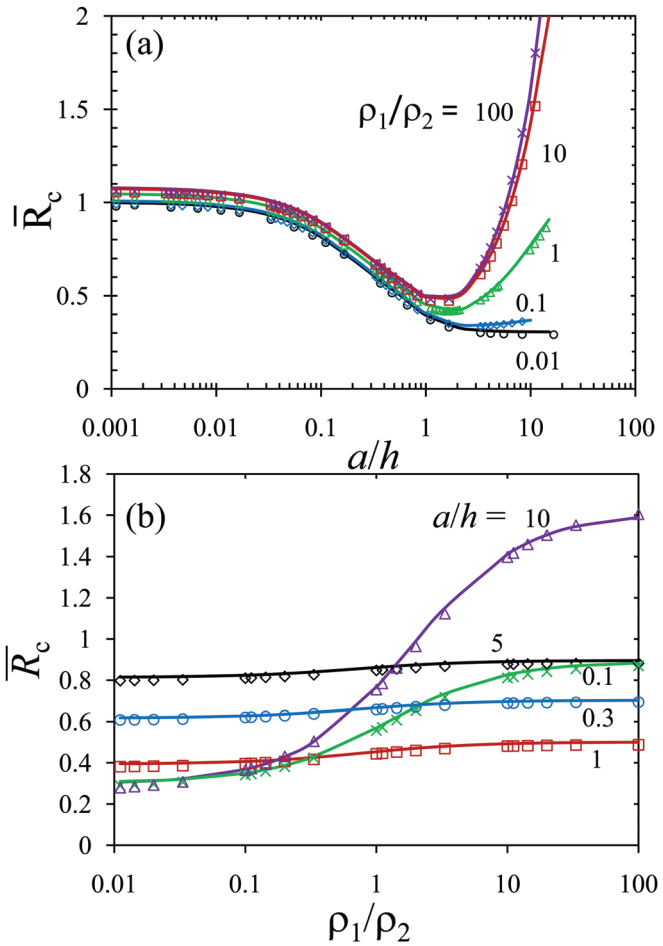

FIG. 11. (Color online) $\bar{R}_c$ for cylindrical thin film structures in Figs. 1 and 3, as a function of (a) aspect ratio a/h, and (b) resistivity ratio ρ_1/ρ_2; symbols for the exact theory, solid lines for the scaling law Eq. (11).

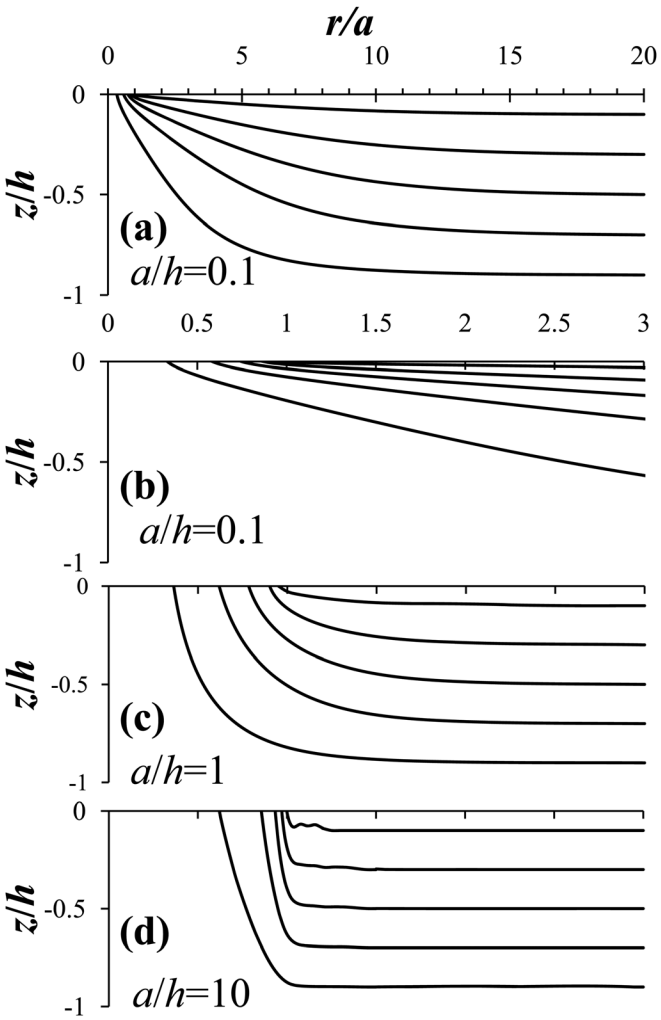

FIG. 12. Field lines in the right half of Region II of the cylindrical geometry in Fig. 1 for $\rho_1/\rho_2 = 1$ with (a) $a/h = 0.1$, (b) zoom in view of (a) for $0 \le r/a \le 3$, (c) $a/h = 1$, and (d) $a/h = 10$.

This scaling law of cylindrical thin film contact resistance, Eq. (11), is shown in Fig. 11, which compares very well with the exact theory, for the range of $0 < \rho_1/\rho_2 < \infty$ and $0.001 \le a/h < 10$. (We have not found the scaling law for $a/h > 10$ for general values of ρ_1/ρ_2, as explained in the preceding paragraph.)

Similar to the Cartesian case, the field lines in the thin film region are calculated from Eq. (B1), by numerically solving the field line equation $dz/dr = (\partial\Phi_-/\partial z)/(\partial\Phi_-/\partial r)$. Figure 12 shows the field lines in the right half of Region II (Fig. 1) for the special case of $\rho_1/\rho_2 = 1$, with various aspect ratios a/h. It is clear that the field lines are most uniformly distributed over the conduction region when $a/h = 1$, which is consistent with the smallest normalized contact resistance $\bar{R}_c$ near $a/h = 1$ for $\rho_1/\rho_2 = 1$ (Figs. 10 and 11). The field lines are horizontally crowded around the corner of the constriction when $a/h \ll 1$ [Fig. 12(b)], and become vertically crowded around the corner when $a/h \gg 1$ [Fig. 12(d)], leading to higher contact resistance in both limits, in the same manner as already explained for the Cartesian case. In Fig. 13, the field lines are shown for the special case of $a/h = 1$, with various resistivity ratios ρ_1/ρ_2. As ρ_1/ρ_2 increases, Region II becomes more conductive relative to Region I, the interface between Regions I and II (i.e., *BC* in Fig. 1) becomes more and more like equipotential, therefore, the field lines (and the current density) at the interface become more uniformly distributed, as shown in Fig. 13(c).

IV. CONCLUDING REMARKS

This paper presents accurate analytic models which allow ready evaluation of the contact resistance or constriction resistance of thin film contacts with dissimilar materials over a large range of parameter space. We show the large distortions of the field lines as a result of film thickness. The models assume arbitrary aspect ratios, and arbitrary resistivity ratios in the different regions for both Cartesian and cylindrical geometries. From the large parameter space surveyed, it is found that, at a given resistivity ratio, the thin film contact resistance primarily depends only on the ratio of constriction size (a) to the film thickness (h), as long as either $L_2 \gg a$ or $L_2 \gg h$. In the latter cases, the electrostatic fringe field is restricted to the constriction corner only, and becomes insensitive to the location of terminals for the thin film region.

The effects of dissimilar materials are summarized as follows. If the constriction size (a) is small compared to the film thickness (h), the thin film contact resistance is insensitive to the resistivity ratio. However, if $a/h > 1$, the contact resistance varies significantly with the resistivity ratio.

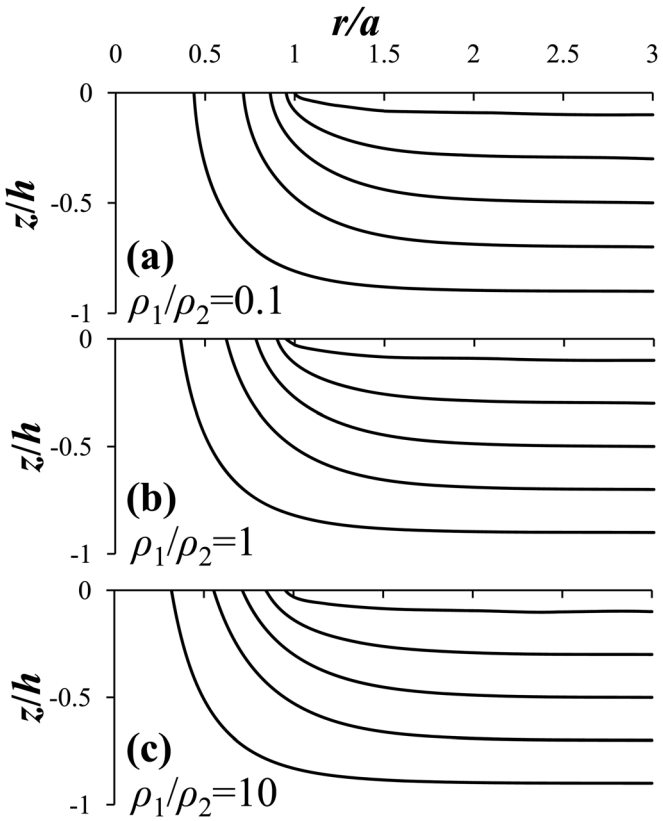

FIG. 13. Field lines in the right half of Region II of the cylindrical geometry in Fig. 1 for $a/h=1$ with (a) $\rho_1/\rho_2=0.1$, (b) $\rho_1/\rho_2=1$, and (c) $\rho_1/\rho_2=10$.

Typically the minimum contact resistance is realized with $a/h\sim 1$, for both Cartesian and cylindrical cases. Various limiting cases are studied and validated with known results. Accurate analytical scaling laws are presented.

Finally, one may adapt the results in this paper to the steady state heat flow in thermally insulated thin film structures with dissimilar thermal properties. This may be done with Fig. 1 by replacing the electrical conductivity $(1/\rho_j)$ with the thermal conductivity (κ_j), $j=1, 2$, in the different regions, assuming that the κ_j's are independent of temperature.

APPENDIX A: THE CONTACT RESISTANCE OF CARTESIAN THIN FILM

Referring to Fig. 1, we assume that $L_1 \gg a$, so that the current flow is uniform at the end GH, far from the joint region. For the two dimensional Cartesian channel, the y-axis and z-axis are in the plane of the paper. The solutions of Laplace's equation are

$$\Phi_+(y,z) = A_0 + \sum_{n=1}^{\infty} A_n \cos\left(\frac{n\pi y}{a}\right) e^{-\left(\frac{n\pi z}{a}\right)} - E_{+\infty} z, \quad z>0, |y|\in(0,a),$$

$$\Phi_-(y,z) = V_0 + \sum_{n=1}^{\infty} \left[B_n \sinh\left(\frac{(n-1/2)\pi z}{b}\right) + C_n \cosh\left(\frac{(n-1/2)\pi z}{b}\right)\right] \cos\left(\frac{(n-1/2)\pi y}{b}\right), \quad z<0, |y|\in(0,b), \tag{A1}$$

where Φ_+ and Φ_- are the electrical potential in the region $BCHG$ and $BCEF$, respectively, $E_{+\infty}$ is the uniform electric fields at the end GH, V_0 is the electrical potential at the ends E and F $(y=\pm b)$, and A_n and B_n are the coefficients that need to be solved.

Since the current flows parallel to the thin film boundary EF, we have

$$\frac{\partial \Phi_-}{\partial z} = 0, \quad z=-h, |y|\in(0,b), \tag{A2}$$

which leads to

$$C_n = B_n \coth\left(\frac{(n-1/2)\pi h}{b}\right). \tag{A3}$$

At the interface $z=0$, from the continuity of electrical potential and current density, we have the following boundary conditions:

$$\Phi_+ = \Phi_-, \quad z=0, |y|\in(0,a), \tag{A4a}$$

$$\frac{1}{\rho_1}\frac{\partial \Phi_+}{\partial z} = \frac{1}{\rho_2}\frac{\partial \Phi_-}{\partial z}, \quad z=0, |y|\in(0,a), \tag{A4b}$$

$$\frac{\partial \Phi_-}{\partial z} = 0, \quad z=0, |y|\in(a,b). \tag{A4c}$$

From Eqs. (A4a) and (A1), the coefficient A_n is expressed in terms of B_n

$$A_0 = \sum_{n=1}^{\infty} B_n \coth\left(\frac{(n-1/2)\pi h}{b}\right) \frac{\sin[(n-1/2)\pi a/b]}{(n-1/2)\pi a/b} + V_0, \tag{A5a}$$

$$A_n = \sum_{m=1}^{\infty} B_m \coth\left(\frac{(m-1/2)\pi h}{b}\right) g_{mn},$$

$$g_{mn} = \frac{2}{a}\int_0^a \cos\left(\frac{n\pi y}{a}\right)\cos\left(\frac{(m-1/2)\pi y}{b}\right) dy, \quad n\geq 1 \tag{A5b}$$

Combining Eqs. (A3), (A4b), (A4c), and (A5b), we obtain

$$B_n + \frac{1}{n-1/2}\frac{\rho_2}{\rho_1}\sum_{m=1}^{\infty}\gamma_{nm} B_m \coth\left[\frac{(m-1/2)\pi h}{b}\right] = \frac{2}{(n-1/2)\pi}\frac{\rho_2}{\rho_1}\frac{\sin[(n-1/2)\pi a/b]}{(n-1/2)\pi a/b}, \quad n=1,2,3\ldots \tag{A6}$$

where

$$\gamma_{nm} = \gamma_{mn} = \sum_{l=1}^{\infty} l g_{nl} g_{ml}, \tag{A7}$$

and g_{nl} and g_{ml} is in the form of the last part in Eq. (A5b). Note that in deriving Eq. (A6), we have set $aE_{+\infty}=-1$ for simplicity. It can be shown from Eq. (A6) that $B_n \propto 1/n^2$ as $n\to\infty$ (c.f., Appendix B of Ref. 15). Thus, by writing Eq.

(A6) in an infinite matrix format, B_n can be solved directly with guaranteed convergence.

The total resistance from EF to GH is $R=(\Phi_F - \Phi_G)/I=V_0/I$, where $I=|2aW(E_{+\infty}/\rho_1)|=2W/\rho_1$ is the total current in the conducting channel, and W is the channel width in the third, ignorable dimension that is perpendicular to the paper. The contact resistance, R_c, is the difference between the total resistance R and the bulk resistance (exterior to $ABCD$) $R_u=\rho_1 L_1/2aW+\rho_2 L_2/2hW$. From Eq. (A1) and (A5a), we find

$$R_c=\frac{|A_0-V_0|}{I}-\frac{\rho_2 L_2}{2hW}=\frac{\rho_2}{4\pi W}\bar{R}_c,$$

$$\bar{R}_c=\bar{R}_c\left(\frac{a}{b},\frac{a}{h},\frac{\rho_1}{\rho_2}\right)=2\pi\frac{\rho_1}{\rho_2}\sum_{n=1}^{\infty}B_n\coth[(n-1/2)\pi h/b]\times\frac{\sin[(n-1/2)\pi a/b]}{(n-1/2)\pi a/b}-\frac{2\pi(b-a)}{h}, \tag{A8}$$

which is the *exact* expression for the contact resistance of Cartesian thin film of dissimilar materials (Fig. 1) for arbitrary values of a, b ($b>a$), h, and ρ_1/ρ_2. It appears in Eq. (1) of the main text. Given the resistivity ratio ρ_1/ρ_2 and aspect ratios a/h and a/b, the coefficient B_n is solved numerically from Eq. (A6), $\bar{R}_c$ is then obtained from Eq. (A8).

In the limit of $\rho_1/\rho_2\to\infty$, Eq. (A6) may be simplified to

$$B_n=\frac{2}{(n-1/2)\pi}\frac{\rho_2}{\rho_1}\frac{\sin[(n-1/2)\pi a/b]}{(n-1/2)\pi a/b},\quad n=1,2,3... \tag{A9}$$

Thus, from Eq. (A8), $\bar{R}_c$ is found as

$$\bar{R}_c\left(\frac{a}{b},\frac{a}{h}\right)=4\sum_{n=1}^{\infty}\frac{\coth[(n-1/2)\pi h/b]}{n-1/2}\frac{\sin^2[(n-1/2)\pi a/b]}{[(n-1/2)\pi a/b]^2}-2\pi(b-a)/h,\ \rho_1/\rho_2\to\infty, \tag{A10}$$

which appears as Eq. (2) in the main text.

APPENDIX B: THE CONTACT RESISTANCE OF THIN FILM TO ROD GEOMETRY

Referring to Fig. 1, similar to the Cartesian case, we also assume that $L_1\gg a$, so that the current flow is uniform at the end GH, far from the joint region. The solutions of Laplace's equation in the cylindrical geometry are[9,15]

$$\Phi_+(r,z)=A_0+\sum_{n=1}^{\infty}A_nJ_0(\alpha_n r)e^{-\alpha_n z}-E_{+\infty}z,\quad z>0,r\in(0,a);$$

$$\Phi_-(r,z)=V_0+\sum_{n=1}^{\infty}\left[B_n\sinh\left(\frac{\lambda_n z}{b}\right)+C_n\cosh\left(\frac{\lambda_n z}{b}\right)\right]\times J_0\left(\frac{\lambda_n r}{b}\right),\quad z<0,r\in(0,b), \tag{B1}$$

where Φ_+ and Φ_- are the electrical potential in the region $BCHG$ and $BCEF$, respectively, $E_{+\infty}$ is the uniform electric fields at the end GH, V_0 is the electrical potential at the thin film rim E and F ($r=b$), $J_0(x)$ is the zeroth order Bessel function of the first kind, α_n and λ_n satisfy $J_1(\alpha_n a)=J_0(\lambda_n)=0$, and A_n and B_n are the coefficients that need to be solved.

Since the current flows parallel to the thin film boundary EF, we have

$$\frac{\partial\Phi_-}{\partial z}=0,\quad z=-h,r\in(0,b), \tag{B2}$$

which leads to

$$C_n=B_n\coth\left(\frac{\lambda_n h}{b}\right). \tag{B3}$$

At the interface $z=0$, from the continuity of electrical potential and current density, we have the following boundary conditions:

$$\Phi_+=\Phi_-,\quad z=0,r\in(0,a), \tag{B4a}$$

$$\frac{1}{\rho_1}\frac{\partial\Phi_+}{\partial z}=\frac{1}{\rho_2}\frac{\partial\Phi_-}{\partial z},\quad z=0,r\in(0,a), \tag{B4b}$$

$$\frac{\partial\Phi_-}{\partial z}=0,\quad z=0,r\in(a,b). \tag{B4c}$$

From Eqs. (B1) and (B4a), the coefficient A_n is expressed in terms of B_n

$$A_0=\sum_{n=1}^{\infty}B_n\coth\left(\frac{\lambda_n h}{b}\right)\frac{2J_1(\lambda_n a/b)}{\lambda_n a/b}+V_0, \tag{B5a}$$

$$A_n=\sum_{m=1}^{\infty}B_m\coth\left(\frac{\lambda_m h}{b}\right)g_{mn},$$

$$g_{mn}=\frac{2}{a^2J_0^2(\alpha_n a)}\int_0^a rdrJ_0(\alpha_n r)J_0\left(\frac{\lambda_m r}{b}\right),\quad n\geq 1. \tag{B5b}$$

Combining Eqs. (B3), (B4b), (B4c), and (B5b), we obtain

$$B_n+\frac{\rho_2}{\rho_1}\frac{a}{b}\frac{1}{\lambda_n J_1^2(\lambda_n)}\sum_{m=1}^{\infty}\gamma_{nm}B_m\coth\left(\frac{\lambda_m h}{b}\right)=\frac{\rho_2}{\rho_1}\frac{2J_1(\lambda_n a/b)}{\lambda_n^2 J_1^2(\lambda_n)},\quad n=1,2,3..., \tag{B6}$$

where

$$\gamma_{nm}=\gamma_{mn}=\sum_{l=1}^{\infty}g_{nl}g_{ml}\alpha_l aJ_0^2(\alpha_l a), \tag{B7}$$

and g_{nl} and g_{ml} is in the form of the last part in Eq. (B5b). Note that in deriving Eq. (B6), we have set $aE_{+\infty}=-1$ for simplicity. It can be shown from Eq. (B6) that $B_n\propto 1/\lambda_n^2\propto 1/n^2$ as $n\to\infty$ (c.f., Appendix A of Ref. 15). Thus, by writing Eq. (B6) in an infinite matrix format, B_n can be solved directly with guaranteed convergence.

The total resistance from EF to GH is $R=(\Phi_F - \Phi_G)/I=V_0/I$, where $I=\left|\pi a^2(E_{+\infty}/\rho_1)\right|=\pi a/\rho_1$ is the total current in the conducting channel. The contact resistance, R_c, is the difference between the total resistance R and bulk resistance (exterior to $ABCD$) $R_u=\rho_1 L_1/\pi a^2+(\rho_2/2\pi h)\ln(b/a)$. From Eq. (B1) and (B5a), we find

$$R_c = \frac{|A_0 - V_0|}{I} - \frac{\rho_2}{2\pi h}\ln\left(\frac{b}{a}\right) = \frac{\rho_2}{4a}\overline{R}_c,$$

$$\bar{R}_c\left(\frac{a}{b},\frac{a}{h},\frac{\rho_1}{\rho_2}\right) = \frac{8}{\pi}\frac{\rho_1}{\rho_2}\sum_{n=1}^{\infty} B_n \coth(\lambda_n h/b)\frac{J_1(\lambda_n a/b)}{\lambda_n a/b} - \frac{2a}{\pi h}\ln\left(\frac{b}{a}\right), \quad \text{(B8)}$$

which is the *exact* expression for the contact resistance between a thin film and a coaxial rod of dissimilar materials (Fig. 1) for arbitrary values of a, b $(b>a)$, h, and ρ_1/ρ_2. It appears in Eq. (7) of the main text. Given the resistivity ratio ρ_1/ρ_2 and aspect ratios a/h and a/b, the coefficient B_n is solved numerically from Eq. (B6), $\overline{R}_c$ is then obtained from Eq. (B8).

In the limit of $\rho_1/\rho_2 \to \infty$, Eq. (B6) may be simplified to

$$B_n = \frac{\rho_2}{\rho_1}\frac{2J_1(\lambda_n a/b)}{\lambda_n^2 J_1^2(\lambda_n)}, \qquad n = 1, 2, 3... \quad \text{(B9)}$$

Thus, from Eq. (B8), $\overline{R}_c$ is found as

$$\overline{R}_c\left(\frac{a}{b},\frac{a}{h}\right) \cong \frac{16}{\pi}\sum_{n=1}^{\infty}\frac{J_1^2(\lambda_n a/b)}{\lambda_n a/b}\frac{\coth(\lambda_n h/b)}{\lambda_n^2 J_1^2(\lambda_n)} - \frac{2a}{\pi h}\ln(b/a), \quad \rho_1/\rho_2 \to \infty, \quad \text{(B10)}$$

which appears as Eq. (9) in the main text.

ACKNOWLEDGMENTS

This work was supported by an AFOSR grant on the Basic Physics of Distributed Plasma Discharges, L-3 Communications Electron Device Division, and Northrop-Grumman Corporation. One of us (P.Z.) gratefully acknowledges a fellowship from the University of Michigan Institute for Plasma Science and Engineering.

[1]G. H. Gelinck, T. C. T. Geuns, and D. M. de Leeuw, Appl. Phys. Lett. **77**, 1487 (2000); W. J. Greig, *Integrated Circuit Packaging, Assembly and Interconnections* (Springer, New York, 2007).
[2]J. L. Carbonero, G. Morin, and B. Cabon, IEEE Trans. Microwave Theory Tech. **43**, 2786 (1995).
[3]P. M. Hall, Thin Solid Films **1**, 277 (1967); *ibid.* **300**, 256 (1997).
[4]H. Klauk, G. Schmid, W. Radlik, W. Weber, L. Zhou, C. D. Sheraw, J. A. Nichols, and T. N. Jackson, Solid-State Electronics **47**, 297 (2003).
[5]R. H. Baughman, A. A. Zakhidov, and W. A. de Heer, Science **297**, 787 (2002).
[6]D. Shiffler, T. K. Statum, T. W. Hussey, O. Zhou, and P. Mardahl, in *Modern Microwave and Millimeter Wave Power Electronics*, edited by R. J. Barker, J. H. Booske, N. C. Luhmann, and G. S. Nusinovich (IEEE Press, Piscataway, NJ, 2005), Chap. 13, p. 691; V. Vlahos, J. H. Booske, and D. Morgan, Appl. Phys. Lett. **91**, 144102 (2007).
[7]W. Wu, S. Krishnan, T. Yamada, X. Sun, P. Wilhite, R. Wu, K. Li, and C. Y. Yang, Appl. Phys. Lett. **94**, 163113 (2009); Z. Yao, C. L. Kane, and C. Dekker, Phys. Rev. Lett. **84**, 2941 (2000); D. Mann, A. Javey, J. Kong, Q. Wang, and H. Dai, Nano Lett. **3**, 1541 (2003).
[8]R. Miller, Y. Y. Lau, and J. H. Booske, Appl. Phys. Lett. **91**, 074105 (2007).
[9]R. Timsit, Proc. of the 54th IEEE Holm Conf. on Electrical Contacts, pp. 332-336 (2008); M. B. Read, J. H. Lang, A. H. Slocum, and R. Martens, Proc. of the 55th IEEE Holm Conf. on Electrical Contacts, pp. 303-309 (2009); G. Norberg, S. Dejanovic, and H. Hesselbom, IEEE Trans. Compon. Packag. Technol. **29**, 371 (2006).
[10]D. A. Chalenski, B. R. Kusse, and J. B. Greenly, Phys. Plasmas **16**, 082707 (2009); M. R. Gomez, J. C. Zier, R. M. Gilgenbach, D. M. French, W. Tang, and Y. Y. Lau, Rev. Sci. Instrum. **79**, 093512 (2008).
[11]R. Holm, *Electric Contacts,* 4th ed. (Springer-Verlag, Berlin, 1967).
[12]R. S. Timsit, IEEE Trans. Compon. Packag. Technol. **22**, 85 (1999); A. M. Rosenfeld and R. S. Timsit, Quart. Appl. Math. **39**, 405 (1981).
[13]Y. Y. Lau and W. Tang, J. Appl. Phys. **105**, 124902 (2009).
[14]M. R. Gomez, D. M. French, W. Tang, P. Zhang, Y. Y. Lau, and R. M. Gilgenbach, Appl. Phys. Lett. **95**, 072103 (2009).
[15]P. Zhang and Y. Y. Lau, J. Appl. Phys. **108**, 044914 (2010). There is a typo in this paper. In Eq.(6) of this paper, the term -2.2281$(a/b)^2$ in $g(b/a)$ should read -1.2281$(a/b)^2$.
[16]M. W. Denhoff, J. Phys. D: Appl. Phys. **39**, 1761 (2006).
[17]P. Zhang, Y. Y. Lau, and R. M. Gilgenbach, Appl. Phys. Lett. **97**, 204103 (2010).
[18]See http://www.ansoft.com for MAXWELL 3D software.